Bull. Chem. Soc. Ethiop. **2027**, 41(1), 55-68.
DOI: https://dx.doi.org/10.4314/bcse.v41i1.5

ISSN 1011-3924
Printed in Ethiopia
Online ISSN 1726-801X
© 2027 Chemical Society of Ethiopia and The Authors

BINDING OF CITROMYCETIN WITH BIVALENT METALS IN SOLVENTS: DFT, REACTIVITY ANALYSIS, SOLVENT EFFECTS, DOCKING AND MD INVESTIGATIONS

Jamelah S. Al-Otaibi[1], Y. Sheena Mary[2*], J.B. Bhagyasree[3], Asmita Mondal[4], Nivedita Acharjee[4], Maria Cristina Gamberini[5]

[1]Department of Chemistry, College of Science, Princess Nourah Bint Abdulrahman University, P.O. Box 84428, Riyadh 11671, Saudi Arabia
[2]Department of Physics, FMN College, Kollam, Kerala, University of Kerala, India
[3]Department of Polymer Chemistry, Government College Attingal, University of Kerla, Thiruvananthapuram, Kerala, India
[4]Department of Chemistry, Durgapur Government College, J. N. Avenue, Paschim Bardhaman, Durgapur, West Bengal, India
[5]Department of Life Sciences, University of Modena and Reggio Emilia, via G. Campi 103, 41125 Modena, Italy

(Received September 8, 2025; Revised March 5, 2025; Accepted September 17, 2026)

ABSTRACT. Citromycetin (DOCA), a structurally well-characterized frequentic acid derivative, can act as a bidentate ligand in coordination with metal ions. In this work, the complexation behavior of DOCA with Cd, Cu, Mg, Ni, Pb, and Zn was systematically investigated using density functional theory (DFT), molecular docking, and molecular dynamics (MD) simulations. The calculated binding energies and thermochemical parameters indicate the formation of stable DOCA–metal complexes and reveal differences in metal binding affinity. The results show that the interaction patterns of DOCA with Cd, Cu, Mg, and Zn are relatively similar, whereas Ni and Pb exhibit distinct coordination behavior. Non-covalent interaction (NCI) analysis further confirms the presence of strong attractive interactions within the complexes. The influence of solvent environments (water, DMSO, and ethanol) on the stability and solvation behavior of DOCA and its metal complexes was also investigated through solvation free energy calculations, revealing more favorable stabilization in water and ethanol than in DMSO. In addition, docking and MD simulations were performed to examine the interaction of the most favorable complexes with the target protein and to evaluate their structural stability during binding. This study provides new insights into the stability, electronic properties, and interaction characteristics of DOCA–metal complexes, contributing to a better understanding of their coordination behavior and potential biological interactions.

KEY WORDS: DFT, Frequentic acid, Metal binding, Solvation energies, MD simulations

INTRODUCTION

Metal coordination compounds derived from biologically active organic ligands have attracted considerable attention because metal complexation can significantly modify the structural, electronic, spectroscopic, and biological properties of the parent molecules [1-3]. Transition- and alkaline-earth-metal complexes have been extensively investigated for their applications in medicinal chemistry, catalysis, sensing, and materials science owing to their diverse coordination geometries and tunable physicochemical properties [4-7]. Among various heterocyclic scaffolds, chromene and coumarin derivatives have emerged as important pharmacophores exhibiting antioxidant, antimicrobial, anti-inflammatory, and anticancer activities [8]. Their multiple donor atoms enable efficient coordination with metal ions, often resulting in complexes with altered stability and biological performance. Consequently, understanding the coordination chemistry of

*Corresponding author. E-mail: ysheenamary@gmail.com
This work is licensed under the Creative Commons Attribution 4.0 International License

chromene-based ligands has become increasingly important for the rational design of functional metal complexes [9, 10].

Density functional theory (DFT) has become a powerful tool for investigating the structural and electronic properties of coordination compounds [11, 12]. In combination with molecular docking and solvation analyses, DFT provides detailed insight into molecular geometry, charge distribution, frontier molecular orbitals, global reactivity descriptors, and solvent-dependent stability, thereby complementing experimental studies and facilitating the prediction of molecular behavior in biological environments. In particular, solvent effects play an important role because they directly influence molecular stability, electronic structure, and intermolecular interactions, which ultimately affect the physicochemical and biological properties of metal complexes [13, 14].

Citromycetin (DOCA), a chromene-derived frequentic acid derivative, contains carbonyl and hydroxyl functional groups capable of coordinating with metal ions, making it a promising ligand for coordination chemistry. Although chromene-based metal complexes have been widely reported, systematic computational studies examining the coordination behavior of DOCA with different metal ions, together with the influence of solvent environments on their stability, electronic properties, and biological interaction potential, remain scarce. Furthermore, comparative investigations combining DFT calculations, solvation free-energy analysis, thermodynamic evaluation, and molecular docking for DOCA-metal complexes have not been comprehensively reported. This lack of molecular-level understanding limits the rational assessment of how different metal ions modify the physicochemical characteristics and potential biological relevance of DOCA.

To address this gap, the present work investigates the coordination behavior of DOCA with Cd, Cu, Mg, Ni, Pb, and Zn, representing metal ions with diverse electronic configurations and coordination characteristics. Geometry optimization, electronic structure analysis, global reactivity descriptors, vibrational characterization, thermodynamic properties, and solvent effects in water, DMSO, and ethanol were evaluated using DFT calculations. In addition, molecular docking simulations were performed to assess the interaction potential of the complexes with biological targets. By integrating quantum chemical calculations, solvation analysis, and docking studies, this work provides a comprehensive molecular-level understanding of the influence of metal coordination and solvent environment on the stability, electronic properties, and potential biological behavior of DOCA complexes, thereby providing useful insights for the future design of chromene-based metal-containing therapeutic and functional materials.

Methods

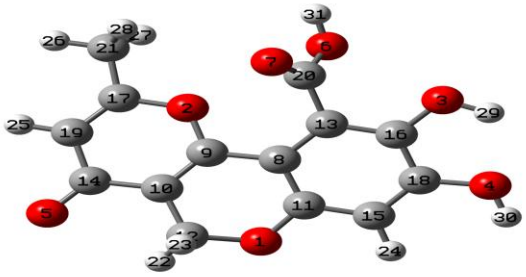


Figure 1 Optimized geometry of DOCA

For optimization of DOCA (Figure 1) and metal-coordinated DOCA, Gaussian16 and GaussView were used [15, 16]. Metal atoms (Cd/Cu/Mg/Ni/Pb/Zn) are attached to oxygen atoms O3 and O4, and all the structures are optimized for a minimum energy configuration. Analysis of FMO distributions as well as ESP was done to better understand electrical properties [17]. For

calculations, the B3LYP/LANL2DZ was used. The CPCM was used to calculate energies of aqueous solutions [18]. The reactivity analysis was done using Multiwfn software [19]. VMD software [20] was used to visualize the ESP and NCI isosurfaces. ELF was visualized by UCSF Chimera [21].

Docking was done with PDBs 6MF4 and 2KCE for the systems due to the anticancer activity of the title compound. In this case, MD simulation for 100 ns was performed using the Desmond software package to evaluate RMSD, Rg, and H-bonds [22].

The present investigation is entirely theoretical and does not involve the experimental synthesis or physicochemical characterization of the proposed DOCA–metal complexes. All molecular structures were constructed computationally and optimized using density functional theory (DFT) to investigate their structural, electronic, thermodynamic, solvation, and molecular interaction properties. The calculated results are intended to provide predictive insights into the coordination behavior and stability of these complexes and to serve as a theoretical foundation for future experimental synthesis and spectroscopic validation.

RESULTS AND DISCUSSION

Solvation effects

The free energy that results from transfer of a molecule between gas and solvent is known as solvation free energy (SFE). SFEs can help us understand how a solvent responds to various surroundings as well as how much a molecule favors one phase over another. For instance, the inherent asymmetry of water causes it to solvate molecules of opposing polarity differently; surfaces also have symmetric effects on ion sharing that rely on surface and environment influences on the solvation of hydrophobic compounds [23, 24]. Solvation free energy of DOCA is -17.17, -9.16, and -17.60 kcal/mol in water, DMSO, and ethanol (Table 1). Even though all of the results were negative, comparing them to the expected SFE values shows that, with the exception of DMSO, all solvents may be preferable for solubilizing DOCA. Although experimental solubility data for DOCA in water and ethanol are not available, the calculated solvation free energies suggest slightly higher solubility in ethanol, consistent with the preferential stabilization of hydrophobic and aromatic moieties in less polar solvents. Since most bioorganic processes occur in solvent environments, particularly aqueous media, the higher stability predicted by the SFE in solvents other than DMSO may suggest improved compatibility with biological environments. In all metal complexes, solvation energy is also lower in DMSO than in the case of the parent molecule. Maximum solvation energies for DOCA-Cd/Mg/Zn in water and ethanol. The thermochemical quantities in Table S1 show that the changes are great. Entropy changes are positive for all metal complexes during the process. Additionally, the change in free energy (ΔG) for Cu/Ni suggested that the event occurred spontaneously. In the case of DOCA-Mg, the changes are positive. Also, ΔS of DOCA with metals was calculated.

Table 1. Solvation energies DOCA in solvents.

System	Solvation energy (kcal/mol)		
	Water	DMSO	Ethanol
DOCA	-17.17	-9.16	-17.60
DOCA-Cd	-71.58	-46.61	-82.24
DOCA-Cu	-48.02	-36.34	-45.87
DOCA-Mg	-71.55	-52.40	-66.17
DOCA-Ni	-33.04	-22.29	-30.65
DOCA-Pb	-28.69	-16.50	-26.04
DOCAZn	-90.15	-60.64	-82.74

Reactivity studies

The conceptual DFT was used to compute reactivity descriptors. The stability of a molecule can be inferred from hardness, and a large energy gap increases stability [25]. Also, organisms with low electrophilicity and potential values can be classified as nucleophilic, whereas electrophiles often have high electrophilicity and potential values. Domingo et al. classified compounds with $\omega < 0.8$ eV as weak, those with $0.8 < \omega < 1.5$ as moderate, and those with $\omega > 1.5$ eV as strong electrophiles [26].

In vacuum, due to the coordination of metal atoms, the energy gap of all DOCA-metal systems decreases from 3.9172 (DOCA) to the range 1.2511 (minimum for Cd) to 3.0556 (maximum for Cu) (Table S2). Correspondingly, hardness decreases, and the chemical potential and electrophilicity index increase for all DOCA-metal systems. For metal-DOCA systems, the electrophilicity index increases to high values except for Cu and Pb-DOCA systems. In all the solvents, the energy gap and hardness of DOCA and DOCA-metal systems increase, with the maximum changes for DOCA-Mg in DMSO and DOCA-Pb in ethanol and water. For DOCA and DOCA-Ni systems, hardness is minimum, resulting in a high electrophilicity index showing more bioactivity [27].

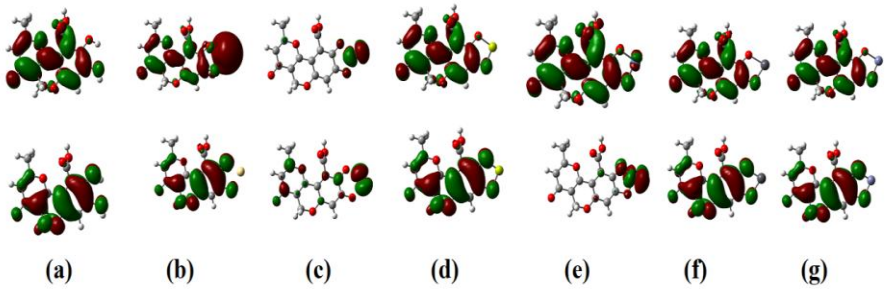


Figure 2. HOMO-LUMO plots: (a) DOCA (b) DOCA-Cd (c) DOCA-Cu (d) DOCA-Mg (e) DOCA-Ni (f) DOCA-Pb (g) DOCA-Zn.

FMOs (Figure 2) are over the entire DOCA except on CH3. In DOCA-Cd, HOMO over the molecule, except on Cd and CH_3, LUMO over the molecule except CH_3 and CH_2; In DOCA-Cu, FMOs are over the Cu atom alone; In DOCA-Mg HOMO and LUMO throughout the system except of Mg and CH_3; in DOCA-Ni, HOMO is over the Ni atom while LUMO on entire molecule except CH_3; in DOCA-Pb/Zn, HOMO and LUMO over the molecule, except Ni and CH_3.

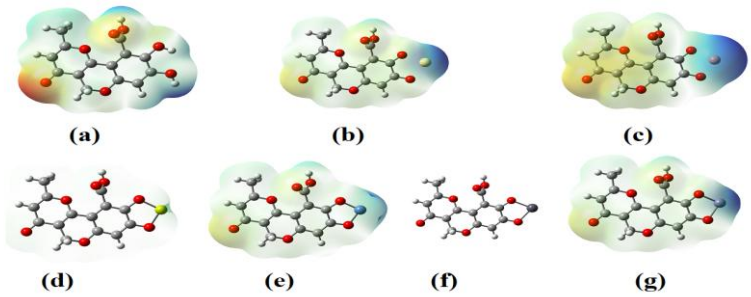


Figure 3. MEP plots (a) DOCA (b) DOCA-Cd (c) DOCA-Cu (d) DOCA-Mg (e) DOCA-Ni (f) DOCA-Pb (g) DOCA-Zn.

Most reactive sites are identified from the MEP plots (Figure 3); in DOCA, O atoms red and yellow; all hydrogen atoms blue. Cd/Cu/Ni/Zn, in addition to the above reactive sites, all the metal atoms are blue, showing more activity. In DOCA-Mg/Pb, the reactivity decreases, with blue only on Mg and no activity of Pb. This means the potential regions of Mg/Pb approach zero-potential regions [28].

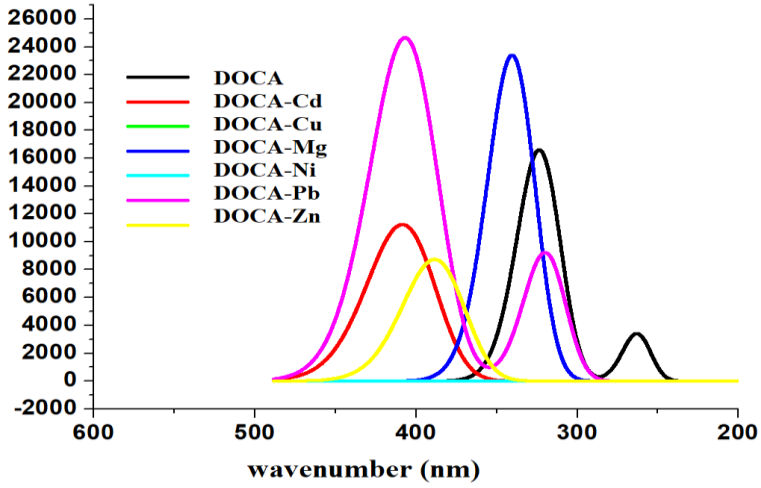


Figure 4. UV-Vis spectra of DOCA and its metal complexes.

The UV-vis of DOCA (Figure 4) are at 262.78 and 324.45 while in DOCA-metals, 408.40, 1043.54 (Cd), 726.92 (Cu), 340.28 (Mg), 418.3 (Ni), 321.54, 406.73 (Pb) and 388.37, 583.04, 1122.33 (Zn). In all metal complexes, there is a very blue shift in the absorption, and for Cd and Zn, in addition to the visible range, there is absorption in the infrared region.

From the theoretically predicted NLO properties (Table S3), the dipole moments and polarizabilities of all metal-DOCA systems are increasing, with the maximum moment for DOCA-Mg (14.0668), polarizability for DOCA-Cd (4.702), and first-order hyperpolarizability for DOCA-Zn (109.37) [40]. For DOCA-Cu, there is a small decrease in the first-order hyperpolarizability (113.116) with respect to that of DOCA (13.179). Due to solvation, the dipole moments of all systems show an increase in value (Table S4).

Hyperconjugative interactions [29] involving oxygen lone pairs are high in DOCA (Table S5), whereas in DOCA-metal systems, the energies decrease due to the presence of the metal atom. In DOCA, the O3 and O4 interaction energies with the C13-C16 and C16-C18 bonds are 26.46 and 23.84 kcal/mol, respectively, while in metal systems, these energies decrease to a minimum, except for Mg/Ni/Pb for the C13-C16 bond and Mg for the C16-C18 bond. In DOCA, the bond lengths (Table S6), C16-O3 and C18-O4, are 1.3894 and 1.4001, while in all DOCA-metal systems, these values decrease, while C16-C18 of DOCA (1.4156) increases in DOCA-Metal systems. Also, the O3-M-O4 distances are in the range 2.2533-1.7975. The C-O stretches of DCOA are 1234 and 1297, while for DOCA-M systems, there is a change in the value due to coordination of the metal (Table S7). Also, the O-M-O frequencies agree with those in the literature [30-32]. Due to metal coordination, the charges of O3 and O4 (-0.7033 and -0.8511) of DOCA are changed in DOCA-metal systems (Table S8). Most of the other charges also show deviations from the pristine values.

AIM topological analysis

Herein, the characterization of the interatomic interactions of the selected bivalent metal atoms: Cd/ Cu/ Mg/ Ni/ Pb and Zn with DOCA in the corresponding complexes has been performed using AIM topological analysis by Bader and coworkers [33]. The QTAIM parameters [349], namely, the total electron density (TED) ρ, the Laplacian of electron density (LED), and LOL, were calculated at bond and ring critical points (BCPs and RCPs) between metal atoms and DOCA [35-38]. The ED was lower than 0.1 e, and LED ($\nabla^2\rho(r_c)$) reveal NCIs [54] at the BCPs and RCPs of metal atom-bonded DOCA, which have been isolated in space using RDG, and their AIM-RDG isosurfaces are shown in Figure 5.

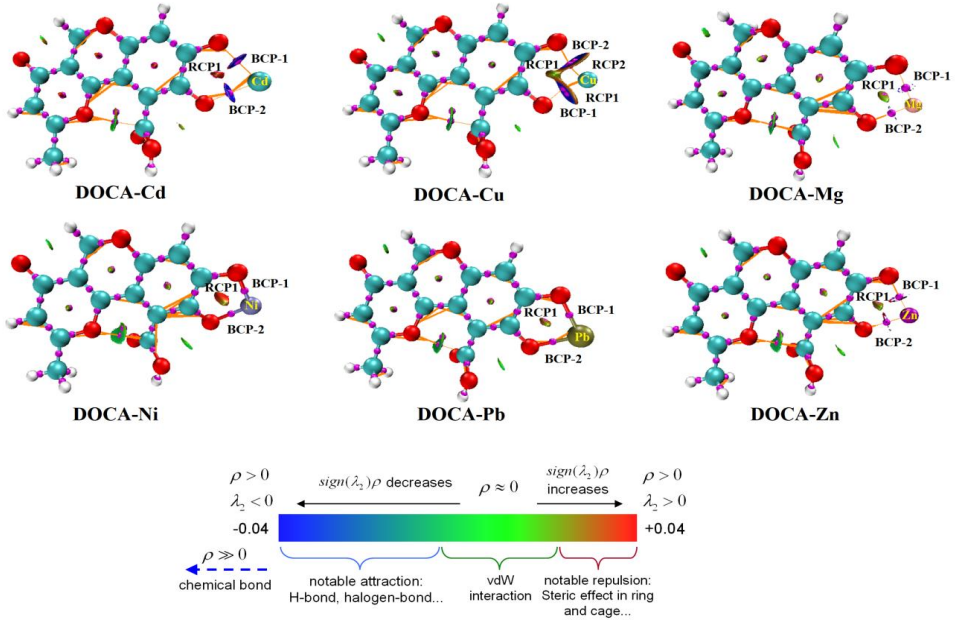


Figure 5. AIM-RDG isosurfaces (isovalue = 0.4), in the range -0.04 <sign(λ_2)ρ< 0.04 a.u. BCPs are shown in magenta and paths in orange.

The AIM study of bivalent metal Cd with DOCA shows two BCPs between the oxygen atoms of DOCA and Cd metal associated with TED ρ 0.053 and 0.054, LED $\nabla^2\rho(r_c)$ 0.314 and 0.319 and LOL of 0.220 and 0.222, respectively, along with one RCP having (ED) ρ 0.018, positive $\nabla^2\rho(r_c)$ 0.092, and LOL of 0.152; indicating NCI, which has been seen as attractive (blue).
Similar to the above study, the bivalent metal Cu with DOCA shows two BCPs between the oxygen of DOCA and Cu metal associated with ρ 0.050 and 0.052, LED $\nabla^2\rho(r_c)$ 0.394 and 0.417, and LOL of 0.170 and 0.171, along with one RCP of total (ED) ρ 0.023, positive $\nabla^2\rho(r_c)$ 0.104 and LOL of 0.176. While another two RCPs between the oxygen atoms of DOCA and Cu metal have ED values of 0.048 and 0.051 and LED values of 0.498 and 0.513, and LOL values of 0.134 and 0.141. respectively; seen attractive (blue) NCIs.
The QTAIM study of the bivalent metal Mg with DOCA shows slightly higher values of the two calculated BCPs between the oxygen atoms of DOCA and Mg metal interacting in a similar way

with the TED ρ 0.062 a.u. and 0.063, positive $\nabla^2\rho(r_c)$ 0.541 and 0.553, and LOL of 0.246 and 0.247. One RCP showing TED ρ 0.018, positive $\nabla^2\rho(r_c)$ 0.104 and LOL of 0.152 have a similarity with that of the above two metal-complex interactions. Non-covalent interactions are indicated as attractive by the blue color.

The study of the bivalent metal Ni with DOCA shows slightly higher values of the two calculated BCPs between the oxygen atoms of DOCA and Ni metal interacting in a similar way with the TED ρ 0.108 and 0.109, LED $\nabla^2\rho(r_c)$ 0.825 and 0.832 and LOL of 0.232 and 0.233. One RCP shows total (ED) ρ 0.031, positive $\nabla^2\rho(r_c)$ 0.165 and LOL of 0.181 have a similarity with that of the above two metal-complex interactions. Non-covalent interactions are indicated, which are weak/strong attractive, as green/blue NCIs.

The study of the bivalent metal Pb with DOCA shows slightly higher values of the two calculated BCPs between the oxygen atoms of DOCA and Pb metal interacting in a similar way with the total (ED) ρ 0.099 and 0.102, LED $\nabla^2\rho(r_c)$ 0.469 and 0.484, and LOL of 0.348 and 0.349. One RCP shows TED ρ 0.023, positive $\nabla^2\rho(r_c)$ 0.143 and LOL of 0.147 have a similarity with that of the above two metal-complex interactions. Non-covalent interactions are indicated, with weak NCIs shown in green and strong ones in blue. The study of the bivalent metal Zn with DOCA shows slightly higher values of the two calculated BCPs between the oxygen atoms of DOCA and Zn metal interacting in a similar way with the total (ED) ρ 0.072 and 0.073, LED $\nabla^2\rho(r_c)$ 0.477 and 0.487, and LOL of 0.249 each, respectively. One RCP showing TED ρ 0.021, positive $\nabla^2\rho(r_c)$ 0.122 and LOL of 0.149 have a similarity with that of the above two metal-complex interactions. NCIs are indicated as strongly attractive by the blue color.

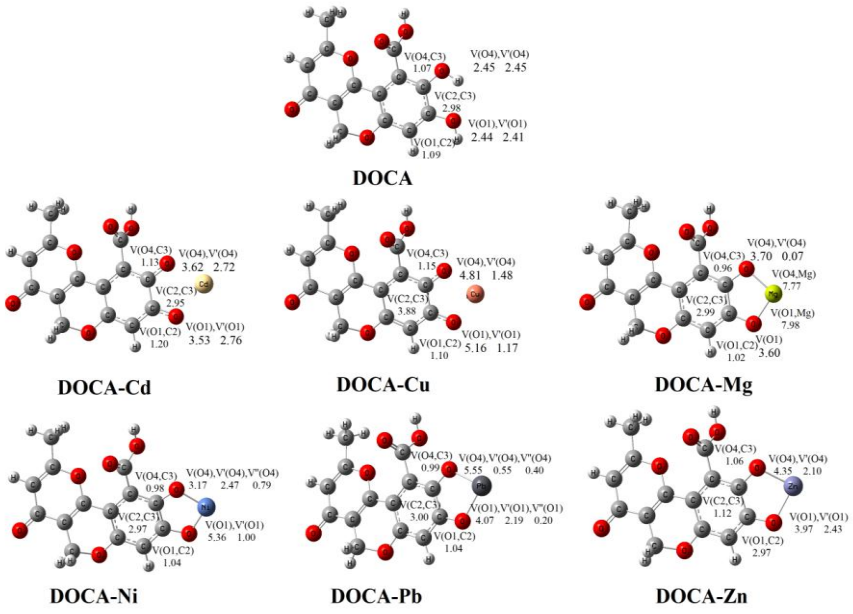


Figure 6. ELF valence basin populations at the drug structure of the studied complexes.

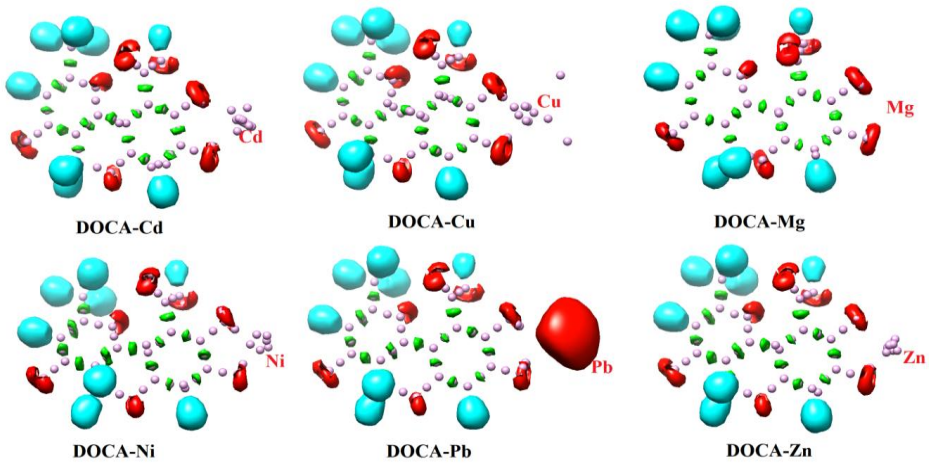


Figure 7. ELF localization domains (Isovalue = 0.85). Protonated basins are shown in blue, monosynaptic basins in red, and disynaptic basins in green colour. The ELF attractor positions are shown as pink spheres.

The ELF analysis was performed to get a mathematical representation of the electronic structure in the studied systems, as shown in Figure 6, along with the ELF domains (Figure 7) [39, 40]. ELF of each structure has V(O1) and V'(O1) basins with the non-bonding electron density (NBED) of O1, integrating population of 4.85 e for DOCA which increases to 6.29 e, 6.33 e, 6.36 e, 6.46 e and 6.40 e in the DOCA-Cd/Cu/Ni/Pb/Zn complexes respectively; except for DOCA-Mg complex in which the total population decreases to 3.60 e due to accumulation of NBED of O atom around Mg metal atom with total population 7.98 e owing to the presence of NCIs. Similarly, each structure has V(O4) and V'(O4) basins with NBED of O4 atom, integrating population of 4.90 e for DOCA are increased to 6.39 e, 6.29 e, 6.43 e, 6.50 e and 6.45 e in the DOCA-Cd/Cu/Ni/Pb/Zn complexes respectively; except for DOCA-Mg complex where the total population decreases to 3.77 e as the NBED of oxygen atom accumulated around Mg metal atom with total population 7.77 e. Thus, from these results, we can conclude that the Mg metal atom shows relatively more influence on the complexation than the other studied metal atoms (Cd/Cu/Ni/Pb/Zn) with the DOCA ligand.

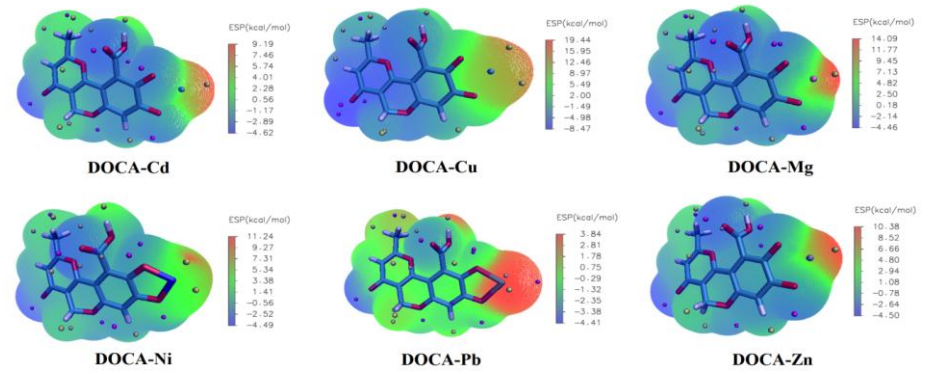


Figure 8. Molecular electrostatic potential (MEP) isosurfaces with the electrostatic potential (ESP) in kcal mol^{-1} of the surface maxima (yellow) and surface minima (magenta).

MEP maps were analyzed to identify the nucleophilic and electrophilic sites in the complex (Figure 8). The surface minima/maxima are shown in magenta/yellow. MEP of DOCA-Cd shows 7/9 minima/maxima with ESP between -4.62 and 9.19. The negative ESP associated with blue regions between -4.62 and -1.17 is throughout the DOCA ligand. Whereas, the Cd metal atom is located around the red region with ESP between 5.74 and 9.19, having traces of green regions with ESP between 0.56 and 4.01.

The MEP of DOCA-Cu gives 4 minima and 10 maxima with ESP values between -8.47 and 19.44. Similar to that of the DOCA-Cd complex, here also the DOCA ligand occupies the negative ESP-associated blue regions between -8.47 and -1.49, while the Cu metal atom occupies the red zone with ESP between 12.46 and 19.44, showing traces of green portions with ESP between 2.00 and 12.46. While the DOCA-Mg gives 7 minima and 10 maxima with ESP values between -4.46 and 14.09. Similar to the above two complexes, the DOCA ligand is located in the blue zones with negative ESP between -4.46 and 0.18, and the Mg metal atom is in the red zone with ESP between 11.77 and 14.09, with traces of green portions with ESP between 0.18 and 9.45.

The DOCA-Ni shows 9 minima and 12 maxima with ESP values between -4.49 and 11.24. The results obtained in this case are quite similar to those of the above-analyzed complexes, except for the positive ESP associated with the red region between 7.31 and 11.24 kcal mol-1, which is present in a very trace amount, while the metal atom Ni is located around the green parts with ESP between 1.41 and 5.34. The negative ESP associated with blue parts between -4.49 and -0.56 is occupied by the DOCA ligand.

The DOCA-Pb complex shows the exact same number of 9 minima and 12 maxima as present in the DOCA-Ni complex, with ESP between -4.41 and 3.84. However, for the DOCA-Pb complex, the MEP analysis is distinctly different from the above observed ones. Herein, the DOCA ligand is located mostly around the green region, with ESP between -2.35 and -0.29, and shades of blue region with negative ESP between -4.41 and -2.35. The Pb metal atom is located around the positive ESP associated with the red regions between 1078 and 3.84.

The DOCA-Cd and DOCA-Zn complexes show similar values of 7 minima and 9 maxima with ESP between -4.50 and 10.38, which is also very close to that of the DOCA-Cd complex. The negative ESP associated with blue shades between -4.50 and -0.78 is occupied by the DOCA ligand. The red regions with ESP between 6.66 and 10.38 are around Zn, with shades of green regions with ESP between 1.08 and 4.80. Note that the DOCA-Cd/Cu/Mg/Zn interactions are quite similar to each other, unlike those of DOCA-Ni/Pb interactions.

Molecular dynamics and docking

The PDBS, 6MF4 [41] and 2KCE [42] are taken for docking (since their binding affinities are high for DOCA-Ni; Table S9 gives binding affinities and Figure S1 provides the amino acid interactions for all complexes) with the systems due to anticancer activity, and AutoDock is used [43-46]. An appropriate technique for investigating the structural dynamics of proteins and their interactions with ligands is the application of all-atom MD simulation. Because it enables a thorough examination of molecular systems at the atomic level, this method has completely transformed the field of drug design and discovery. MD simulations were used in this study to examine the dynamic changes that take place when the target protein binds. The RMSD values were examined over time to look at the stability of the target protein complex and learn more about how the systems behaved (Figure 9). DOCA and Ni were found to have average RMSD values of 4.8Å and 4.1Å respectively.

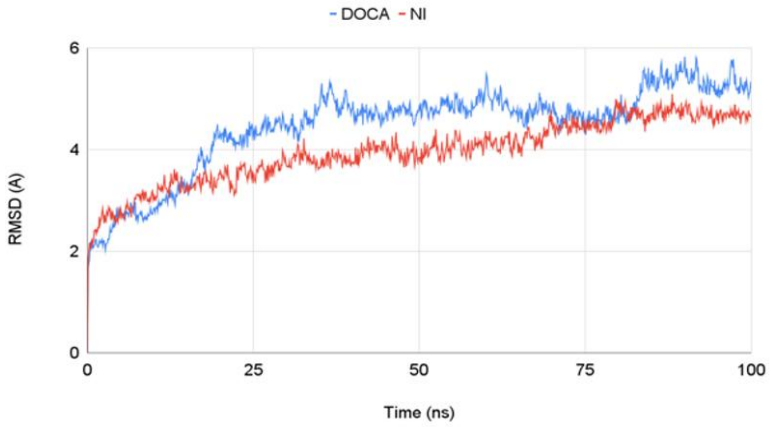


Figure 9. Conformational dynamics of the DOCA- Ni complex: Time evolution of the RMSD values.

The Rg values were calculated and plotted over time to evaluate the dynamic stability and compactness of DOCA and Ni complexes (Figure S2). Ni and DOCA were found to have average Rg values of 19.1 A and 19.2 Å, respectively.

The creation of H-bonds is essential for evaluating the stability of protein-ligand interactions. The time-dependent behavior of the hydrogen bonds between DOCA and Ni was examined in this work, and the findings were plotted (Figure S3) [47-50].

CONCLUSION

This study systematically investigated the coordination behavior and physicochemical properties of DOCA complexes with selected metal ions (Cd, Cu, Mg, Ni, Pb, and Zn) using density functional theory (DFT), solvation analysis, molecular docking, and molecular dynamics simulations. The calculated thermochemical parameters indicate the formation of stable DOCA–metal complexes, with negative free energy changes observed for the Cu and Ni systems, suggesting spontaneous complex formation, whereas the DOCA–Mg complex shows positive thermodynamic values. Solvation free energy analysis reveals that DOCA exhibits favorable solubility in water and ethanol compared to DMSO. Electronic structure analysis shows noticeable spectral shifts upon complex formation. A blue shift in the absorption bands was observed for all complexes, while Cd and Zn complexes exhibited additional absorption in the infrared region. The increase in dipole moment values in solvated systems further indicates enhanced polarity due to solvent interactions. Among the investigated metals, Mg shows relatively stronger influence on the complexation behavior with the DOCA ligand, while docking studies reveal that the Ni complex exhibits the highest binding affinity with the selected biological target. Molecular dynamics simulations further support the structural stability of the DOCA–Ni complex, as indicated by the stable RMSD and radius of gyration values. Overall, the results provide insight into the stability, electronic properties, and interaction behavior of DOCA–metal complexes and highlight the potential of these systems for further studies related to coordination chemistry and possible biological interactions. Although the present findings provide valuable theoretical insights into the coordination chemistry and physicochemical properties of DOCA–metal complexes, experimental synthesis and characterization (e.g., FTIR, UV–Vis, NMR, X-ray diffraction, and elemental analysis) will be necessary to validate the predicted structures and properties.

ACKNOWLEDGEMENTS

Princess Nourah Bint Abdulrahman University Researchers Supporting Project number (PNURSP2026R13), Princess Nourah Bint Abdulrahman University, P.O. Box 84428, Riyadh 11671, Saudi Arabia.

Author contribution

CRediT: Jamelah S.Al-Otaibi: Investigation, Data curation, Software, Supervision, Validation, Visualization, Writing-original draft; Y.Sheena Mary: Methodology, Investigations, Formal analysis, review and editing, Writing-original draft, Writing-review and editing; Asmita Mondal: Investigation, Data curation, Software, Validation, Visualization, Writing-original draft; Nivedita Acharjee: Investigation, Data curation, Software, Validation, Visualization, Writing-original draft; Maria Cristina Gamberini: Methodology, Investigations, Formal analysis, review and editing, Writing-original draft.

Disclosure statement: No potential conflict of interest was reported by the authors.

Data availability statement: Data is available on request.

REFERENCES

1. Klencsar, Z.; Kontos, Z. EPR analysis of Fe^{3+} and Mn^{2+} complexation sites in fulvic acid extracted from lignite. *J. Phys. Chem. A* **2018**, 122, 3190-3203.
2. Li, L.; Qi, G.; Wang, B.; Yue, D.; Wang, Y.; Sato, T. Fulvic acid anchored layered double hydroxides: a multifunctional composite adsorbent for theremoval of anionic dye andtoxic metal. *J. Hazard Mater*. **2018**, 343, 19-28.
3. Kalaiarasi, G.; Rajkumar, S.R.J.; Dharani, S.; Rath, N.P.; Prabhakaran, R. New cationic and neutral copper(II) complexes containing 7-hydroxy-4-oxo-4[H]-chromene derived ONO pincer ligands: Synthesis, characterization and in vitro biological evaluation. *J. Photochem. Photobiol. B: Biol*. **2018**, 180, 77-77.
4. Badawy, M.A.; Mohamed, G.G.; Omar, M.M.; Nassar, M.M.; Kamel, A.B. Synthesis, spectroscopic and thermal characterization of quinoxaline metal complexes. *Eur. J. Chem*. **2010**, 1, 282-288.
5. Creaven, B.S.; Egan, D.A.; Kavanagh, K.; McCann, M.; Noble, A.; Thati, B.; Walsh, M. Synthesis, characterization and antimicrobial activity of a series of substituted coumarin-3-carboxylatosilver (I) complexes. *Inorg. Chim. Acta* **2006**, 359, 3976-3984.
6. Farrusseng, D.; Aguado, S.; Pinel, C. Metal organic frameworks: opportunities for catalysis. *Angew. Chem. Int. Ed*. **2009**, 48, 7502-7513.
7. Moghadam, P.Z.; Li, A.; Wiggin, S.B.; Tao, A.; Maloney, A.G.P.; Wood, P.A.; Ward, S.C.; Fairen-Jimenez, D. Development of a cambridge structural database subset: A collection of metal organic frameworks for the past, present and future. *Chem. Mater*. **2017**, 29, 2618-2625.
8. Catalano, A.; Sinicropi, M.S.; Iacopetta, D.; Ceramella, J.; Mariconda, A.; Rosano, C.; Scali, E.; Saturnino, C.; Long, P. A review on the advancements in the field of metal complexes with Schiff bases as antiproliferative agents. *Appl. Sci.* **2021**, 11, 6027.
9. Mohamdi, M.; Faghih-Mirzaei, E.; Ebhrahimpour, S.Y.; Sheikhshoaie, I.; Haase, W.; Foro, S. Synthesis, spectroscopic studies, DFT calculations, electrochemical evaluation, BSA binding and molecular docking of an aroylhydrazone-based cis-dioxido Mo(VI) complex. *J. Mol. Struct*. **2017**, 1139, 418-429.

10. Khan, K.M.; Ambreen, N.; Hussain, S.; Perveen, S.; Choudhary, M.I. Schiff bases of 3-formylchromone as thymidine phosphorylase inhibitors. *Bioorg.Med. Chem*. **2009**, 17, 2983-2988.
11. Kontogiorgis, C.; Detsi, A.; Hadjipavlou-Litina, D. Coumarin-based drugs: A patent review (2008-present). *Expert. Opin. Ther. Pat*. **2012**, 22, 437-457.
12. Peng, X. M.; Damu, G.L.V.; Zhou, H. Current developments of coumarin compounds in medicinal chemistry. *Curr. Pharm. Des*. **2013**, 19, 3884-3930.
13. Gonzalez-Rodal, D.; Palomino, G.T.; Cabello, C.P.; Perez-Mayoral, E. Amino-grafted Cu and Sc metal-organic frameworks involved in the green synthesis of 2-amino-4H-chromenes, mechanistic understanding. *Micropor. Mesopor. Mater*. **2021,** 323, 111232.
14. Ticknor, K.V.; Vilks, P.; Vandergraaf, T.T. The effect of fulvic acid on the sorption of actinides and fission products on granite and selected minerals. *Appl. Geochem.* **1996**, 11, 555-565.
15. Gaussian 16, Revision A.03, Frisch, M.J.; Trucks, G.W.; Schlegel, H.B.; Scuseria, G.E.; Robb, M.A.; Cheeseman, J.R.; Scalmani, G.; Barone, V.; Petersson, G.A.; Nakatsuji, H.; Li, X.; Caricato, M.; Marenich, A.V.; Bloino, J.; Janesko, B.G.; Gomperts, R.; Mennucci, B.; Hratchian, H.P.; Ortiz, J.V.; Izmaylov, A.F.; Sonnenberg, J.L.; Williams-Young, D.; Ding, F.; Lipparini, F.; Egidi, F.; Goings, J.; Peng, B.; Petrone, A.; Henderson, T.; Ranasinghe, D.; Zakrzewski, V.G.; Gao, J.; Rega, N.; Zheng, G.; Liang, W.; Hada, M.; Ehara, M.; Toyota, K.; Fukuda, R.; Hasegawa, J.; Ishida, M.; Nakajima, T.; Honda, Y.; Kitao, O.; Nakai, H.; Vreven, T.; Throssell, K.; Montgomery Jr, J.A.; Peralta, J.E.; Ogliaro, F.; Bearpark, M.J.; Heyd, J.J.; Brothers, E.N.; Kudin, K.N.; Staroverov, V.N.; Keith, T.A.; Kobayashi, R.; Normand, J.; Raghavachari, K.; Rendell, A.P.; Burant, J.C.; Iyengar, S.S.; Tomasi, J.; Cossi, M.; Millam, J.M.; Klene, M.; Adamo, C.; Cammi, R.; Ochterski, J.W.; Martin, R.L.; Morokuma, K.; Farkas, O.; Foresman, J.B.; Fox, D.J. Gaussian, Inc., Wallingford CT, **2016**.
16. GaussView, Version 6.1, Dennington, R.; Keith, T.A.; Millam, J.M. Semichem Inc., Shawnee Mission, KS, **2016**.
17. Al-Otaibi, J.S.; Mary, Y.S.; Mary, Y.S.; Acharjee, N.; Ullah, Z. DFT, solvation effects, reactivity and SERS analysis on structural, optical and vibrational properties of a biomolecle of pyrimidine derivative adsorbed on metal clusters of Ag/Au/Cu. *J. Indian Chem. Soc*. **2022**, 99, 100753.
18. Cossi, M.; Rega, N.; Scalmani, G.; Barone, V. Energies, structures and electronic properties of molecules in solution with the C-PCM solvation model. *J. Comput. Chem*. **2003**, 24, 669-681.
19. Lu, T.; Chen, F. Multiwfn: A multifunctional wavefunction analyzer. *J. Comp. Chem*. **2012**, 33, 580-592.
20. Humphrey, W.; Dalke, A.; Schulten, K. VMD: Visual Molecular Dynamics. *J. Mol. Graphics*, **1996**, 14, 33.
21. Pettersen, E.F.; Goddard, T.D.; Huang, C.C.; Couch, G.S.; Greenblatt, D.M.; Meng, E.C.; Ferrin, T.E. UCSF Chimera—a visualization system for exploratory research and analysis. *J. Comput. Chem*. **2004**, 25, 1605-1612.
22. Martyna, G.J.; Tobias, D.J.; Klein, M.L. Constant pressure molecular dynamics algorithms. *J. Chem. Phys*. **1994**, 101, 4177-4189.
23. Guthrie, J.P. A blind challenge for computational solvation free energies, introduction and overview. *J. Phys. Chem. B* 20**09**, 113, 4501-4507.
24. Harris, R.C.; Pettitt, B.M. Effects of geometry and chemistry on hydrophobic salvation. *Proc. Natl. Acad. Sci. USA* **2014**, 111, 14681-14686.
25. Chattaraj, P.K.; Chakraborty, A.; Giri, S. Net electrophilicity, *J. Phys. Chem. A* **2009**, 113, 10068-10074.

26. Domingo, L.R.; Aurell, M.J.; Perez, P.; Contreras, R. Quantitative characterization of the global electrophilicity power of common diene/dienophile pairs in Diesl-Alder reactions. *Tetrahedron* **2002**, 58, 4417-4423.
27. Aswathy, V.V.; Alper-Hayta, S.; Yalcin, G.; Mary, Y.S.; Panicker, C.Y.; Jojo, P.J.; Kaynak-Onurdag, F.; Armakovic, S.; Armakovic, S.J.; Yildiz, I.; Van Alsenoy, C. Modification of benzoxazole derivative by bromine-spectroscopic, antibacterial and reactivity study using experimental and theoretical procedures. *J. Mol. Struct*. **2017**, 1141, 495-511.
28. Rani, P.R.K.; Mary, Y.S.; Fernandez, A.; Priya, S.A.; Mary, Y.S.; Thomas, R. Single crystal XRD, DFT investigations and molecular docking study of 2-((1,5-dimethyl-3-oxo—2phenyl-2,3-dihydro-1H-pyrazol-4-yl)amino)naphthalene-1,4-dione as a potential anticancer agents. *Comput. Biol. Chem*. **2019**, 78, 153-164.
29. Glendening, E.D.; Reed, A.E.; Carpenter, J.E.; Weinhold, F. NBO version 3.1, Gaussian Inc., Pittsburg, PA, 2**003**.
30. Kloska, K.A.; Fortenberry, R.C. Gas phase spectra of MgO molecules: A possible connection from gas phase molecules to planet formation. *MNRAS* **2018**, 474, 2055-2063.
31. Chen, L.; Xu, C.; Zhang, X. F. DFT calculations of vibrational spectra and nonlinear optical properties for MgO nanotube clusters. *J. Mol. Struct. THEOCHEM*. **2008**, 863, 55-59.
32. Canepa, P.; Ugliengo, P.; Alfredsson, M. Elastic and vibrational properties of –α and β-PbO. *J. Phys. Chem. C* **2012**, 116, 21514-21522.
33. Bader, R.F.W. In *Atoms in Molecules: A Quantum Theory*, Oxford, Clarendon Press, **1990**.
34. Bader, R.F.W.; Essén, H. The characterization of atomic interactions. *J. Chem. Phys.* **1984**, 80, 1943-1960.
35. Al-Otaibi, J.S.; Mary, Y.S.; Mary, Y.S.; Mondal, A.; Acharjee, N.; Balachandar, S. Investigation of the adsorption of a DNA based purine derivative on N/B-doped coronene and coronene by means of DFT and NCI interaction analysis. *J. Mol. Liq*. **2022**, 367, 120373.
36. Al-Otaibi, J.S.; Mary, Y.S.; Mary, Y.S.; Mondal, A.; Acharjee, N. DFT analysis on the adsorption of melamine in Ga12-N12/P12 nanocages: Solvent effects, SERS analysis, reactivity properties. *J. Biomol. Struct. Dyn*. **2023**, 41, 8844-8855.
37. Al-Otaibi, J.S.; Mary, Y.S.; Mary, Y.S.; Mondal, A.; Acharjee, N.; Churchill, D.G. Sumanene as a delivery carrier for methimazole drug: DFT, AIM, SERS and solvent effects. *Comput. Theor. Chem.* **2022**, 1215, 113811.
38. Al-Otaibi, J.S.; Mary, Y.S.; Mary, Y.S.; Acharjee, N. Quantum mechanical investigation into the adsorption pattern of clomipramine and methotrimeprazine HCl with graphene and fullerene. *Polycycl. Arom. Compd*. **2022**, 43, 2219-2232.
39. Becke, A.D.; Edgecombe, K.E. A simple measure of electron localization in atomic and molecular systems. *J. Chem. Phys*. **1990**, 92, 5397-5403.
40. Silvi, B.; Savin, A. Classification of chemical bonds based on topological analysis of electron localization functions. *Nature* **1994**, 371, 683-686.
41. Almawi, A.W.; Langloid-Lemay, L.; Boulton, S.; Gonzalez, J.R.; Melacini, G.; D'Amours, D.; Guarne, A. Distinct surfaces on Cdc5/PLK polo-box domain orchestrate combinatorial substrate recognition during cell division. *Sci. Rep*. **2020**, 10, 3379.
42. Rutenber, E.R.; Stroud, R.M. Binding of the anticancer drug ZD1694 to *E.coli* thymidylate synthase: assessing specificity and affinity. *Structure* **1996**, 4, 1317-1324.
43. Morris, G.M.; Huey, R.; Lindstrom, W.; Sanner, M.F.; Belew, R.K.; Goodsell, D.S.; Olson, A.J. AutoDock4 and Autodocktools4; automated docking with selective receptor flexibility. *J. Comput. Chem*. **2009**, 30, 2785-2791.
44. Mary, Y.S.; Panicker, C.Y.; Sapnakumari, M.; Narayana, B.; Sarojini, B.K.; Al-Saadi, A.A.; Van Alsenoy, C.; War, J.A.; Fun, H.K. Infrared spectrum, structural and optical properties and molecular docking study of 3-(4-fluorophenyl)-5-phenyl-4,5-dihydro-1H-pyrazole-1-carbaldehyde. *Spectrochim. Acta* **2015**, 138, 529-538.

45. Demirag, A.D.; Celik, S.; Ozel, A.E.; Akyuz, S. An investigation on the vibrational analysis, molecular structure and interaction with the cellulose enzymes of the cellulose I alpha and cellulose I beta: DFT calculations, docking simulations. *Bull. Chem. Soc. Ethiop.* **2025**, 39, 2041-2064.
46. Durairaju, P.; Raja, G.; Venkatesh, G.; Govindasamy, C.; El Newehy, A.S.; Haseena, S.; Vennila, P.; Balasubramaniyan, S. Green synthesis, characterization, antimicrobial and anti-cancer activity of silver nanoparticles using *Aristolochia bracteolate* plant leaf extract: Experimental and theoretical calculations. *Bull. Chem. Soc. Ethiop*. **2025**, 39, 271-286.
47. Mary, Y.S.; Mary, Y.S.; Armakovic, S.; Armakovic, S.J.; Kratky, M.; Vinsova, J.; Baraldi, C.; Gamberini, M.C. Concentration and solvent dependent SERS, DFT, MD simulations and molecular docking studies of a thioxothiazolidine derivative with antimicrobial properties. *J. Mol. Liq*. **2021**, 329, 115582.
48. Venkatesh, G.; Mammadova, K.; Manikandan, A.; Mary, Y.S.; Vennila, P. Exploring the solvation, structural stability, and molecular interactions of telmisartan: DFT and molecular dynamics simulations, *Bull. Chem. Soc. Ethiop.* **2026**, 40, 893-906.
49. Er. A.; Celik, S.; Ozel, A.E.; Akyuz, S. Detailed insight into the structure and bioactivity of thymocartin, as a potential anticancer and antibacterial agent, through conformational and vibrational analysis, molecular docking, and molecular dynamic studies. *Bull. Chem. Soc. Ethiop.* **2026**, 40, 319-339.
50. Salman, R.H.; Karem, L.K.A. Synthesis and characterization of Mn_3O_4 nanosheets using thyme leaves extract: antibacterial, antioxidant, molecular docking and molecular dynamics studies. *Bull. Chem. Soc. Ethiop.* **2026**, 40, 469-483.